Polymer 50 (2009) 6235–6244

Contents lists available at ScienceDirect

Polymer

journal homepage: www.elsevier.com/locate/polymer

A simple approach to fabricate morphological gradient on polymer surfaces

Shiling Zhang, Bo You, Guangxin Gu, Limin Wu*

Department of Materials Science and the Advanced Coatings Research Center of China Educational Ministry, Advanced Materials Laboratory, Fudan University, Shanghai 200433, PR China

ARTICLE INFO

Article history:
Received 12 September 2009
Received in revised form
23 October 2009
Accepted 2 November 2009
Available online 10 November 2009

Keywords:
Surface morphological gradient
Nanocomposite polymer latex
Film-formation

ABSTRACT

This paper presents a novel and feasible approach for fabrication of morphological gradient surfaces based on the film-formation of nanocomposite polymer latex. In this method, when the polymer latex with relatively low glass transition temperature (T_g) was blended with colloidal silica and then dried at certain temperatures, a morphological evolution with deeper pores from the center to the edge could be directly obtained on polymer surface. Neither careful control of experimental conditions nor any complex processes are needed. The T_g of polymer, the silica content, the solvent and the drying temperature have significant influences on this surface morphology. The film-formation mechanisms at different drying temperatures are also discussed.

1. Introduction

Surface gradient materials [1], of which the surface physical and chemical properties change continuously along the materials, have attracted a lot of interests since this kind of materials represent powerful tools for the rapid, high-throughput investigation and systematic studies of interfacial phenomena in the areas of physics, chemistry, materials and biology [2–7].

Up to now, there are quite several sorts of gradients, such as chemical composition [1,8], density [9] and nanowire length [10], have been experimentally realized through different techniques, including diffusion-controlled vapor deposition [11], cross diffusion [12], plasma or corona treatment [13,14], use of microfluidic devices [15–17], scanning tunneling microscopy [18], spatial gradients of electrochemical potential [10] and physical absorption and chemical reaction on a surface [19–21]. In particular, the last couple of methods are the most widely used for fabrication of gradient surfaces. In the physical absorption approach, an adsorbent, such as a solution of silane, hydrogel or fibronectin, is added to a stationary surface and subsequently absorbed at the surface. Lowering the solution level at a constant rate through a drain changes the time that the given level on the substrate is in contact with solute, resulting in a gradient of adsorbent compound along the length of the stationary surface. Although the technique is simple, it can only be applied to hydrophilic inorganic substrate such as silicon, quartz, or glass. In the method of chemical reaction on a surface, macromolecules or small molecules are bound covalently to a solid surface by either a "grafting to" [20] or "grafting from" [21] approach under controlled conditions, such as continuous variation of temperature, concentration, exposure time or light intensity to fabricate surface-chemical gradients.

Recently, more researches are focusing on the fabrication of surface morphological gradients since surface microstructure also has a huge impact on the surface performances of materials. For example, Tsai and co-workers [22] prepared polymer surfaces with a gradual variation of topography using phase separation of a homopolymer blend and microphase separation of a diblock copolymer. Lu and co-workers [23] fabricated morphological gradients by first creating a porous polyethylene (PE) sheet, and then placing the substrate onto a heating stage with a temperature gradient ranging from 0 °C to temperatures above the melting point of PE. The morphology changed gradually from porous to smooth across the substrate. Zhang and co-workers [24] fabricated a microstructure gradient on polystyrene (PS) surface by heating one side of the close-packed multilayer PS microspheres and keeping another side at room temperature, the PS microspheres changed gradually to a flat PS surface. Very recently, they successfully prepared the textured gradient PS surface by first creating a microrod-structured PS surface using porous anodic aluminum oxide membrane as a template, followed by heating in a gradient temperature field [7]. Other reports include use of the combination of particle erosion with a subsequent chemical polishing step [25], or the influence of surface energy on polymer-blend phase separation [26], and so on [27]. However, it is regretful that most of these methods are to fabricate stochastic surface morphological gradient, and need to accurately control gradient

* Corresponding author. Tel.: +86 21 6511 2075; fax: +86 21 6510 3056.
E-mail address: lmw@fudan.edu.cn (L. Wu).

0032-3861/$ – see front matter © 2009 Elsevier Ltd. All rights reserved.
doi:10.1016/j.polymer.2009.11.003

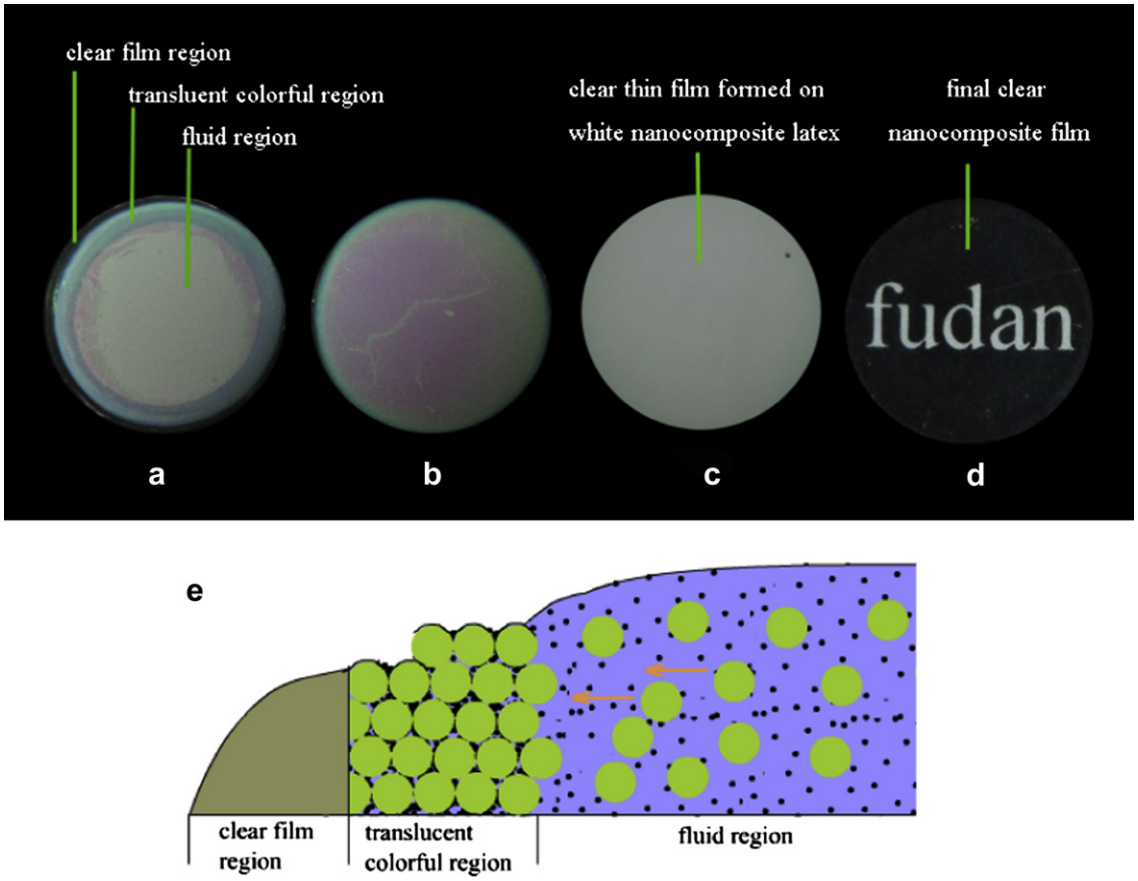

Fig. 1. Digital camera images of the nanocomposite film during the drying process ($T_g = 22$ °C): (a) dried at 40 °C for 15 min, (b) dried at 110 °C for 5 s, (c) dried at 110 °C for 1 min. (d) final clear nanocomposite film, (e) schematical illustration of the three distinct regions in (a).

parameters such as temperatures [7,23,24], properties of the substrates [26] to achieve morphological gradient surfaces.

Recently, we reported a novel and simple method to fabricate ordered porous structure [28–30]. In that approach, a polymer/colloidal silica nanocomposite latex was first prepared by *in-situ* emulsion polymerization or blending method, and then forced-drying to form film at a relatively high temperature (e.g., around 100 °C or higher), a two-dimensional or three-dimensional ordered porous film could be directly obtained. In this study, we further dry the nanocomposite polymer latex at relatively low temperatures, it is surprising to find that a morphological gradient can directly form on the surface, neither careful controlling experimental conditions nor any complex processes are needed.

2. Experimental section

2.1. Materials

Monomers: methyl methacrylate (MMA), butyl acrylate (BA), acrylic acid (AA), were purchased from Sinopharm Chemical Reagent Corp. Auxiliary monomers: allyloxy hydroxypropyl sodium sulfonate (HAPS, 40 wt% of solid content in aqueous solution) was kindly donated by Shuangjian Trading Corp., Ltd. (China). Colloidal silica: Bindzil 2034DI (20 nm, pH = 3, solid content = 34 wt%, zeta potential = −11.1 mV) was provided by Eka Chemicals Corp. (Sweden). Initiator: ammonium persulfate (APS) was purchased from Shanghai Guanghua Chemical Reagent Corp. (China). Ultrapure water (>17 MΩ cm^{-1}) from a Milli-Q water system was used throughout the experiment.

2.2. Synthesis of surfactant-free latex

Poly(MMA-BA-AA) copolymer latex was synthesized by a batch and surfactant-free emulsion polymerization using the following typical procedure and recipe: 0.25 g of HAPS solution and 80 g of deionized water were charged into a 250 mL round bottom flask equipped with a mechanical stirrer, thermometer with a temperature controller, an N_2 inlet, a Graham condenser, and a heating mantle and stirred at room temperature for 15 min. Then, 5 g of monomer mixture was slowly added within 30 min and deoxygenated by bubbling nitrogen gas at room temperature for about 1 h, and heated to 80 °C, followed by addition of aqueous APS solution (0.035 g of APS in 3 g of water). The reaction was conducted at 80 °C for 1.5 h under a slow stream of N_2, and then added by another aqueous APS solution (0.14 g of APS in 12 g of water) and 15 g of monomer mixture over a period of 2 h, and continued to react at 80 °C for another 5 h to obtain polymer latex. Two kinds of polymer latex were synthesized: one (T_g, 46 °C; Mn, 2.5×10^6 and polydispersity, 2.19; mean particle diameter, 366 nm; zeta potential at pH = 5.5, −58.2 mV), and another (T_g, 22 °C; Mn, 3.2×10^6 and Mw/Mn, 2.75; mean particle diameter, 426 nm; zeta potential at pH = 5.5, −51.0 mV) were from the weight ratios of 60:40 and 50:50 for MMA to BA, respectively, other parameters equal.

2.3. Preparation of gradient surface

The gradient surface was prepared by drying the nanocomposite polymer latex at relatively low temperatures. For a typical procedure, the as-prepared polymer latexes or their dispersions in

methanol or methanamide after dialyzed against methanol and methanamide using a cellulose membrane, respectively, were diluted with corresponding solvents to 15 wt% of solid content, then 5 g of the diluted polymer latex was blended with 0.33 g of silica sol under magnetic stirring for 1 h to obtain nanocomposite dispersions. An amount of the freshly prepared nanocomposite was transferred by a micropipette and spread with the pipet tip onto a round glass slide with a diameter of 9 mm, which was placed horizontally in an oven to minimize the disturbance caused by convection during the self-assembly process. When the slides cast with nanocomposites were dried at desired temperature for 24 h, surface morphological gradients were directly obtained. The silica content in the nanocomposite films was 15 wt% based on polymer, except other noted. The thickness of all films was about 70 μm.

2.4. Characterization

Scanning electron microscopy (SEM) images were obtained using a field emission microscope (Philips XL 30, Philips Corp. Holland) operated at an accelerating voltage of 10 kV, the samples

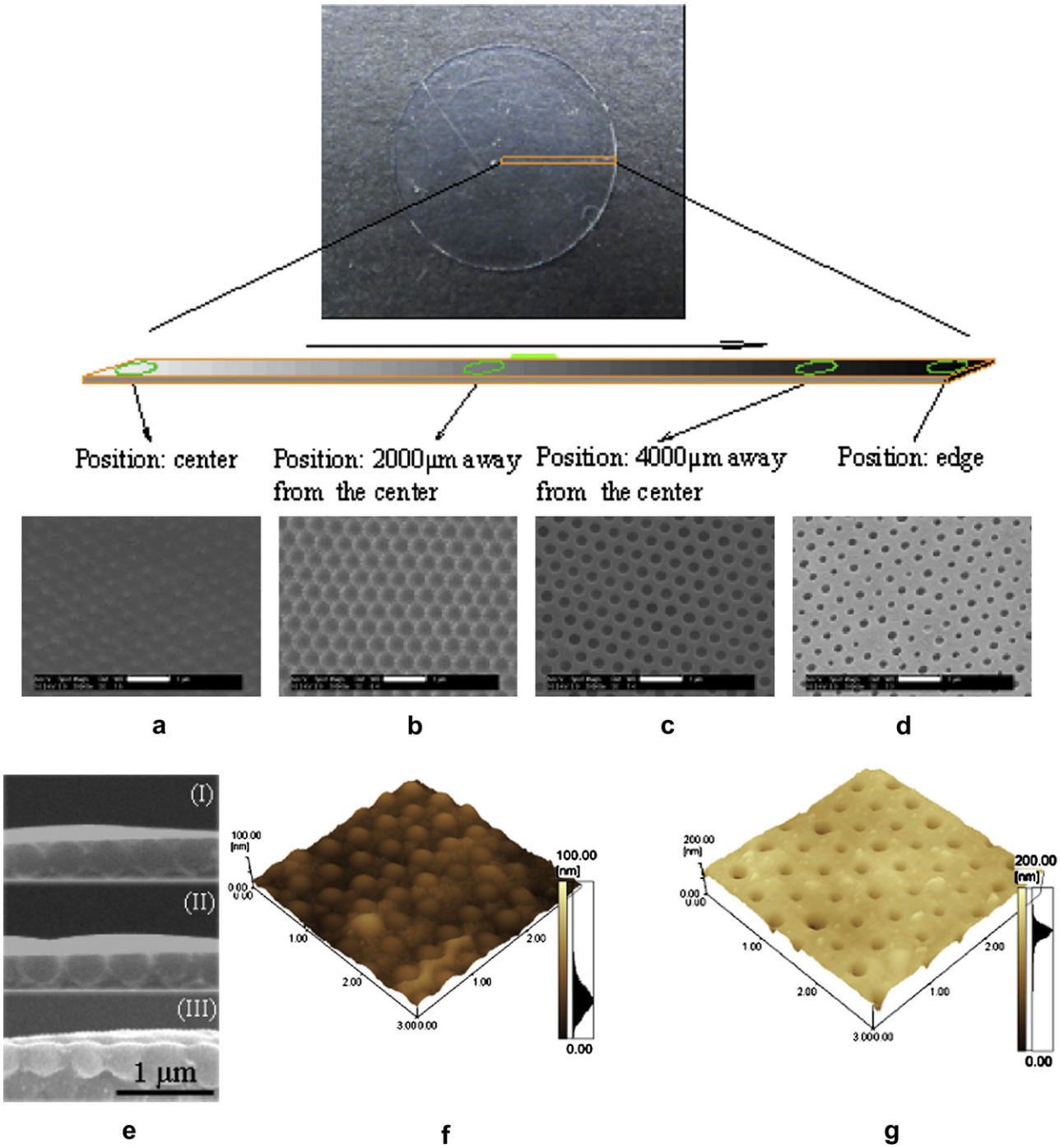

Fig. 2. Surface SEM images of the nanocomposite film along the radius of film ($T_g = 22$ °C, dried at 25 °C). (a) central region, (b) 2 mm away from the center, (c) 4 mm away from the center, (d) edge of the nanocomposite film. All scale bars are 1 μm. (e) Typical cross-sectional SEM images of the film at different positions: (I) edge, (II) 4 mm away from center, (III) center. Typical. AFM images: (f) central region, (g) edge of the nanocomposite film.

were sputter-coated with a thin layer of gold prior to examination. To observe the cross-sectional images, the samples were fractured in liquid nitrogen. Atomic force microscopy (AFM, SPM-9500J3, Shimadz Corp.) images were recorded in tapping mode. X-ray photoelectron spectroscopy (XPS) detection was performed by an ESCA system (PHI 5000 C, Perkin–Elmer, USA) using Al K_α radiation (1486.6 eV) at power of 250 W, and at a take-off angle of 54° with respect to the sample plane. All the binding energies were calibrated by using the containment carbon (C1s = 284.8 eV), the typical XPS error is less than 0.5 atom%. T_g was determined using a Pyris 1 differential scanning calorimeter (DSC) (Perkin Elmer, Inc.). Size exclusion chromatography (SEC) analysis was measured on a Water

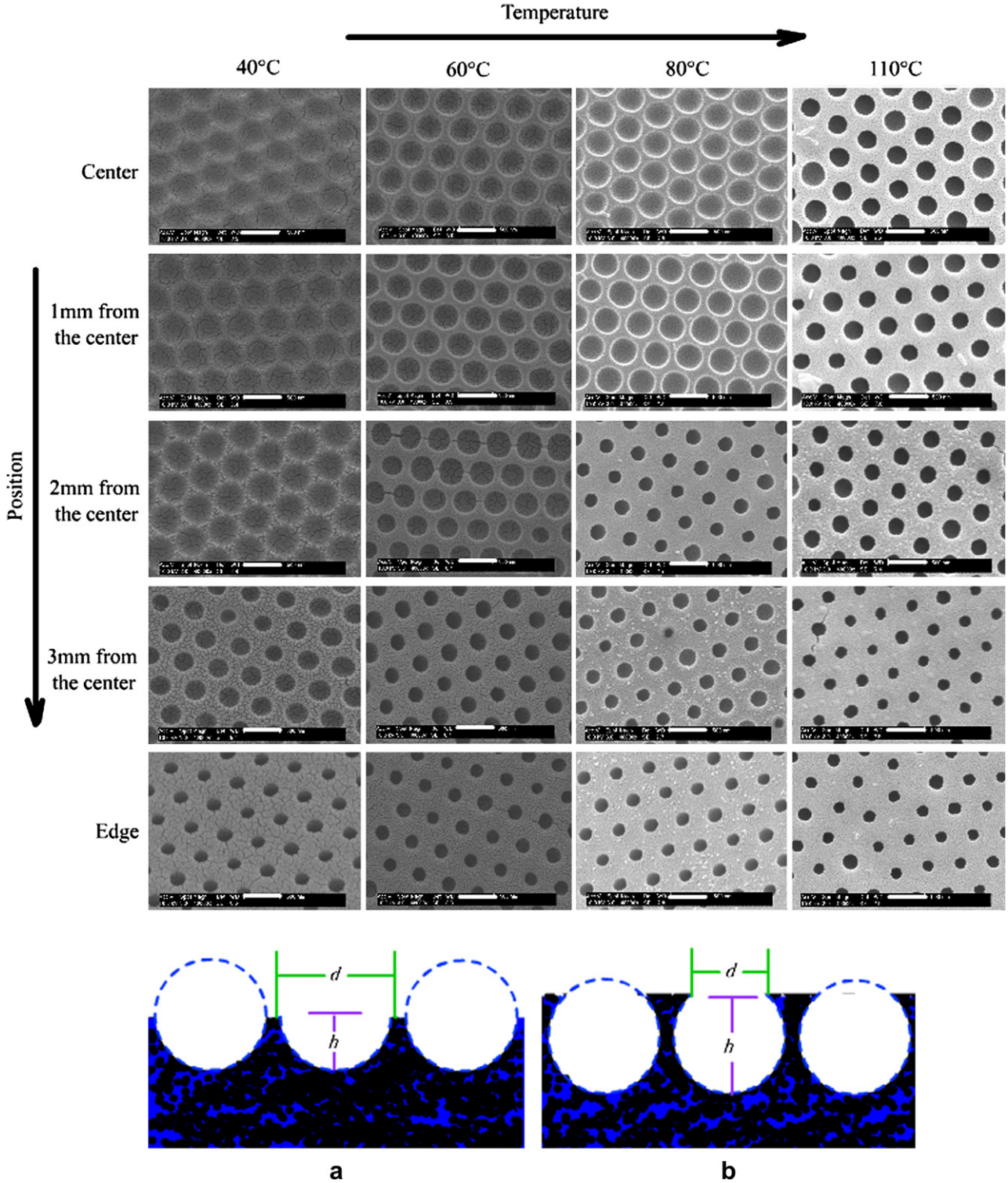

Fig. 3. Top: surface SEM images of the nanocomposite film (from latex with 22 °C of T_g) at different positions. All scale bars are 500 nm. Bottom: illustration of the relationship between the pore morphology and the evaporation rate, (a) relatively low rate and (b) relatively high rate, *d* refers to open pore diameter and *h* to pore depth.

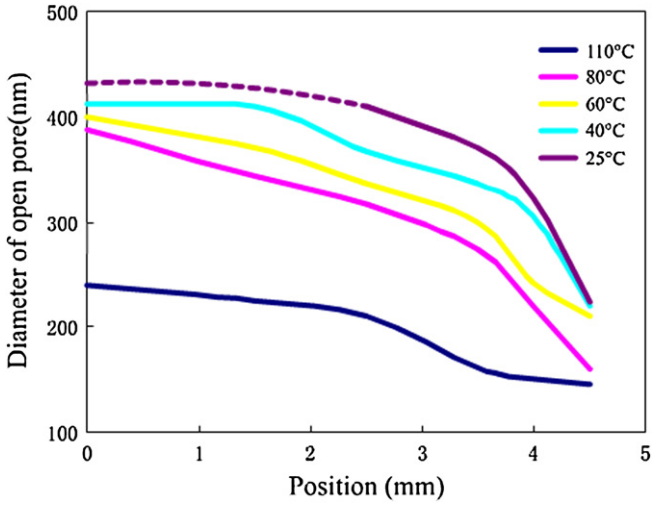

Fig. 4. The pore diameter as functions of position and drying temperature (dashed line represents the periodic arrange of polymer spheres).

system (Waters, USA) with a Water 1515 pump, a Water 2414 refractive index detector, and a set of Styragel columns (HR1, HR3, and HR4) at 35 °C using tetrahydrofuran as an eluent at a flow rate of 1.00 mL/min.

3. Results and discussion

3.1. Apparent morphology change during drying process

The two kinds of nanocomposite polymer latex with different T_g were dried at different temperatures. At relatively low drying temperatures, e. g., 25 °C or 40 °C, the polymer latex with 22 °C of T_g displayed an iridescent color at the edge of the substrate even after several minutes of drying. The typical optical image, as demonstrated in Fig. 1a and schematically illustrated in Fig. 1e, reveals three distinct regions during drying process: the central region with white composite latex, the outermost transparent dried region, and the translucent colorful region separating the aforementioned two regions. As the drying process proceeded, this color gradually moved from the periphery towards the center, while the fluid region shrank and disappeared at the end of drying process, leaving behind a fully transparent film. For the polymer latex with 46 °C of T_g dried at above two temperatures, the nanocomposite latex caused a clear edge with an opaque and cracked film due to high T_g. However, at higher drying temperatures, e. g., 60 °C, 80 °C or 110 °C, both kinds of nanocomposite latex exhibit an iridescent color within a very short time, as shown in Fig. 1b. The higher the drying temperature, the shorter the time to show the color was, and the iridescent color disappeared gradually and a clear thin film formed on white composite latex (Fig. 1c), and finally a whole clear film formed (Fig. 1d).

3.2. Morphological evolution on the film surface

Fig. 2 further presents the surface SEM images of the nanocomposite film prepared from the polymer latex with 22 °C of T_g and 25 °C of drying temperature. It can be seen that the film shows a morphological gradient on the surface along the radius direction. The central region displays a face-center-cubic structure with the periodic arrangement of polymer spheres [30], in which the center-to-center distance between two neighboring spheres is nearly the same as the diameter of the polymer spheres (Fig. 2a). In contrast, the images away from the center indicate highly ordered porous

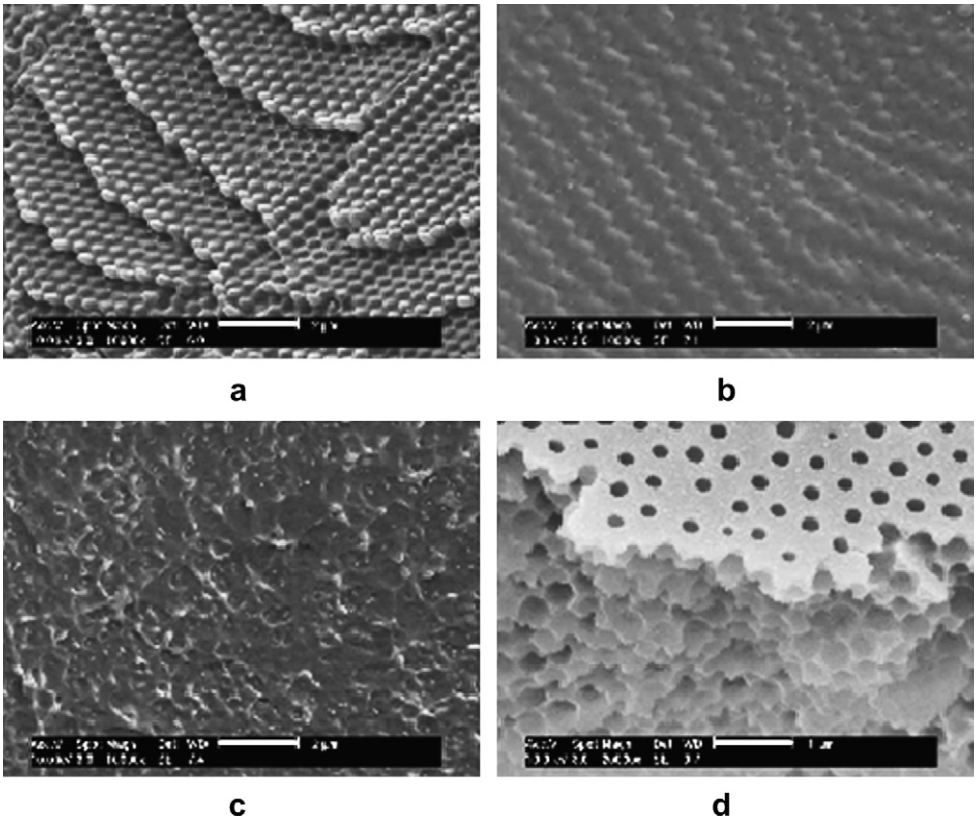

Fig. 5. Typical cross-sectional SEM images of the nanocomposite films (T_g = 22 °C): (a) dried at 40 °C at central region, (b) middle, (c) edge, (d) dried at 110 °C All scale bars are 1 μm.

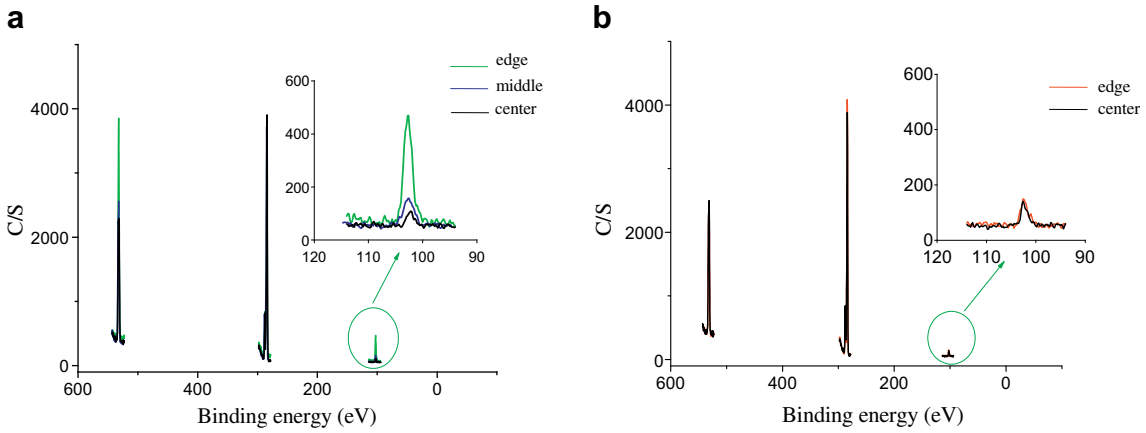

Fig. 6. Typical XPS scans of the nanocomposite films dried at different temperatures ($T_g = 22$ °C): (a) 40 °C, (b) 110 °C.

structure, and the longer the distance away from the central region, the deeper the pores are (Fig. 2b through d). The center-to-center distance between two neighboring pores is also very close to the original size of the polymer spheres, but the pore diameter decreases and the ridge between two neighboring pores increases from the center towards the edge. This porous gradient evolution can be further confirmed by cross-sectional SEM (Fig. 2e) images and AFM images (Fig. 2f and 2g).

When this nanocomposite latex was dried at higher temperatures, e. g., 40 °C, 60 °C, 80 °C and 110 °C, all these films reveal ordered but gradient porous structure, as indicated in Fig. 3. And as the drying temperature increases, the pores are becoming deeper

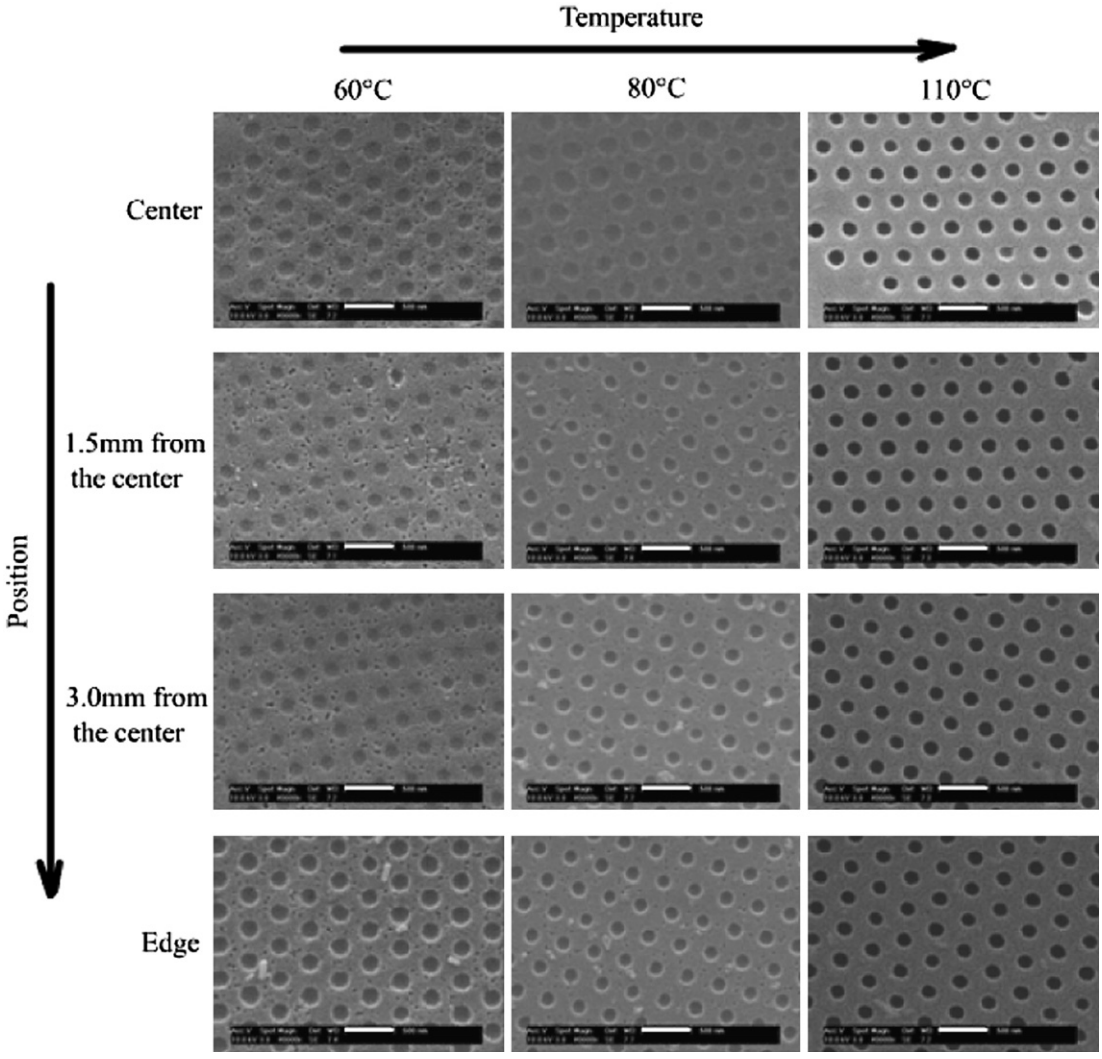

Fig. 7. Surface SEM images of the nanocomposite film from latex with 46 °C of T_g. All scale bars are 1 μm.

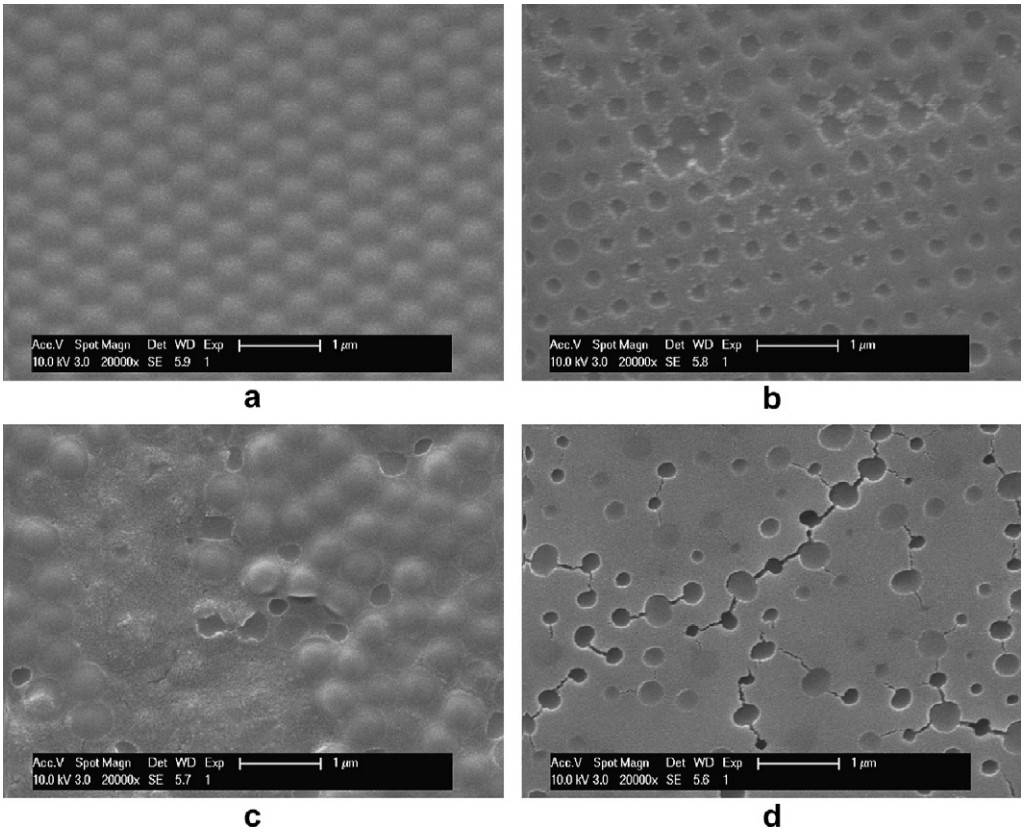

Fig. 8. Surface SEM images of the nanocomposite films with different silica contents: (a) and (b) 5 wt%, (c) and (d) 25 wt%; (a) and (c) central region, (c) and (d) the edge of the film. All scale bars are 1 μm.

but the pore size smaller. The pore diameter as functions of the position and drying temperature is demonstrated in Fig. 4. It clearly shows a gradual decrease in the pore diameter from center towards edge of the sample at all drying temperatures, and higher the drying temperature, the smaller the pore size is. This could be explained as follows: during the drying process, evaporation and convective flow lead to an accumulation of nanoparticles at the air–water interface, increasing the evaporating rate promotes stronger convective flow and more nanoparticles accumulating on the surface, and more polymer spheres moving inside, as shown by schematic diagram in Fig. 3. At the same time, increasing the evaporating rate also results in a higher mobility of polymer chains from the polymer spheres into the voids or interstices between the silica nanoparticles. Thus, higher evaporation rate leads to deeper pores with smaller open pore diameter, and gradual increase of the evaporation rate along the radius from the center to the edge [34] causes a gradient morphology. Also, higher drying temperature provides higher evaporation rate, which is in favor of the formation of pores with smaller open diameter. Thus, the surface morphological evolution can be controlled by tuning the drying temperature.

Fig. 5 further compares the typical cross-sectional SEM images of the films dried at 40 °C and 110 °C. The film dried at 40 °C shows no pores but highly ordered arrangement of polymer spheres at the center of the film (Fig. 5a), these spheres fully deform at the middle and totally coalesce at the edge of the nanocomposite film, even no individual particles can be identified (Fig. 5b and c). However, the film dried at 110 °C displays ordered porous structure in the bulk of the film (Fig. 5d), just as our previous observations [29,30].

Fig. 6 illustrates the typical XPS survey spectra of nanocomposite films dried at 40 °C and 110 °C. Two strong peaks at binding energies of 285 and 535 eV due to C1s and O1s, respectively, can be observed, and the peak at 107 eV attributed to Si2p also exists in all spectra. Furthermore, for the film dried at 40 °C, the inset scans in Fig. 6a show that Si2p peak intensity increases significantly, with the Si atomic percentage increasing from 0.7 at the central region to 5.3 at the edge. While the film dried at 110 °C has comparable Si atomic contents at center (1.1) and edge (1.3). Theoretical Si atomic percent is 4.0 in the composite film. The results indicate that the drying temperature has a great influence on not only on the surface microstructure but also on the surface composition of the composite film.

When the nanocomposite latex prepared from the polymer latex with 46 °C of T_g was dried at 60 °C, 80 °C and 110 °C, all the films unveil periodic porous structure on their surfaces, as illustrated in Fig. 7, but almost no or slight morphological evolution from the center to the edge of film is observed. This could be explained as follows: although the evaporation rate gradient along the radius of the sample still exists, the relatively high T_g significantly slows down the diffusion rate of polymer chains in the polymer spheres, which is not favorable for the formation of gradient surface.

3.3. Effect of silica content on surface morphology

Fig. 8 further demonstrates the typical surface SEM images of the nanocomposite films with various nanosilica contents. At 5 wt% of silica sol, the central region displays a periodic polymer spheres array (Fig. 8a). While shallow and interconnected pores are clearly seen at the edge of the film surface (Fig. 8b), and these pores are somewhat orderly arrayed. This could be due to the insufficient silica particles for the formation of an integrated silica framework. As silica sol was increased to 15 wt%, the surface of the film shows

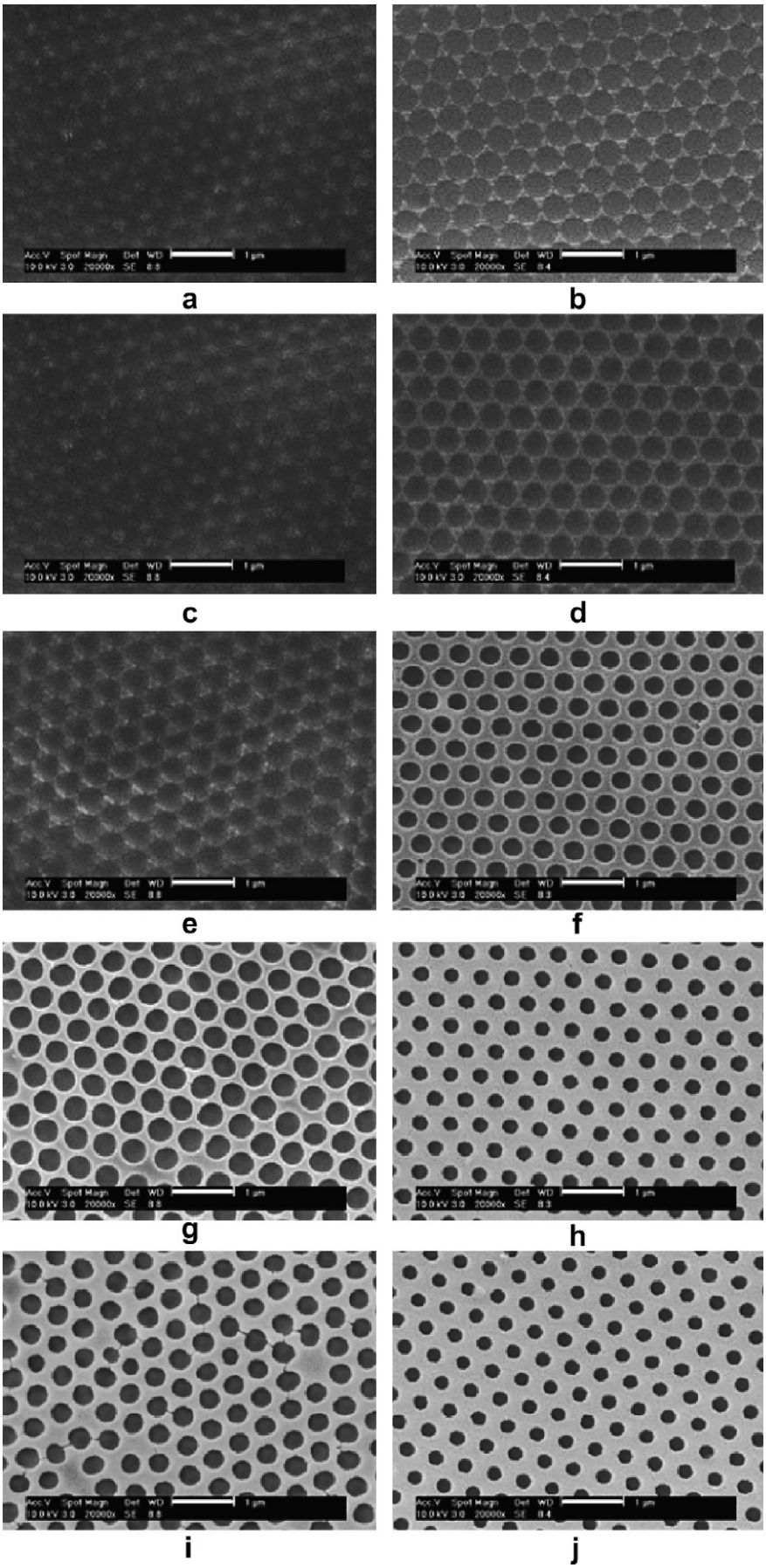

Fig. 9. Surface SEM images of the nanocomposite films prepared in methanol (left column) and methanamide (right column): (a, b) central region, (c, d) 2.0 mm away from the center, (e, f) 3.7 mm away from the center; (g, h) 4.0 mm away from the center, (I, j) the edge of the film. All scale bars are 1 μm.

regular ordered polymer spheres array at the central region (Fig. 2a), and ordered porous structure at the edge of the film (Fig. 2d). As the silica content was further increased to 25 wt%, some polymer spheres are imbedded in the silica particles at the center region of the film (Fig. 8c), and pores could be seen but are locally distributed at the edge of the film (Fig. 8d). These results suggest that 25 wt% of silica sol is already excessive for the formation of an integrated silica framework.

3.4. Effect of solvent on surface morphology

To check the effect of solvent on the surface microstructure of the films, the polymer latex with 22 °C of T_g was dialyzed against methanol, or methanamide using a cellulose membrane to obtain polymer dispersion in methanol or methanamide, and then thoroughly mixed with silica sol by stirring, followed by drying in an oven at 25 °C to form a clear film. Fig. 9 compares the surface morphological evolutions of these films. It can be seen that all these films present a surface morphological gradient along radius direction from center to edge, no matter which solvent was used. However, different solvents have various impacts on the surface microstructure. For the dispersion in methanamide, the film displays shallow cavities even at the central region, while the films from the dispersion in methanol and nanocomposite latex (see Fig. 2) begin to show shallow cavities at around 3.7 mm and 2 mm away from the center, respectively. This should be attributed to the different volatility of the three solvents. Methanamide has the lowest evaporation rate, thus the corresponding dispersion needs to take the longest time for the film-formation, which can provide enough time for silica particles to move towards the top surface. This is favorable for generating pores or cavities. Water has slower volatility than methanol, thus the former avails the system to form cavities or pores than the latter.

3.5. Formation mechanism of the gradient surface

Up to now, there have been developed two typical film-formation mechanisms to explain the crystallization of colloidal particles: one is based on the air–water interface self-assembly via electrostatic interaction and lateral capillary forces [31], another driven by the convective self-assembly mechanism [32,33].

Based on the experimental results and discussion above, we would believe that the convective self-assembly mechanism is dominating the colloidal crystallization at low drying temperature, as depicted in Fig. 10I, while the air–water interface self-assembly mechanism is running the film-formation at relatively high temperatures, as illustrated in Fig. 10II, both of the mechanisms may take place at moderate drying temperatures.

At relatively low drying temperatures, as water or other solvents evaporated, the polymer spheres concentrated first at the edges, and small silica particles immigrated through the channels between polymer spheres to the evaporating menisci and accumulated there, filling in the interspaces between polymer spheres. And the capillary pressure caused by the evaporating menisci formed between particles (polymer spheres and silica nanoparticles) at the packed region, which drew the dispersion from the bulk to the edge, resulting in a lateral front propagation, and three regions: clear film region, saturated solid region and fluid region, as depicted in Fig. 10Ia. Moreover, the evaporation rate at the periphery was higher than that at the center [34], that is, there existed a evaporation rate gradient along the radius of the sample. Since the evaporation and convective flow led to an accumulation of nanoparticles at the surface, and the convective flow was proportional to the pressure difference, which

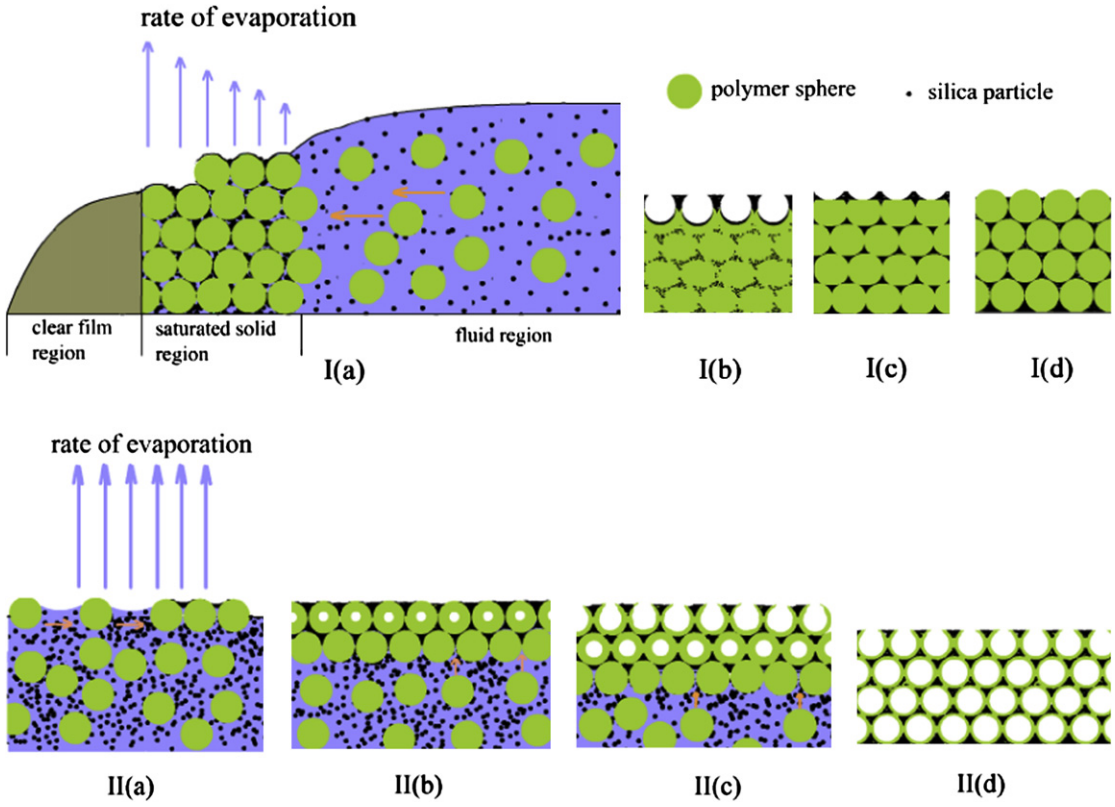

Fig. 10. Possible formation mechanism of the surface morphology of the nanocomposite films dried at (I) low temperature, (II) high temperature. I(a) a composite film containing different regions; I(b) edge, I(c) middle, I(d) center of the film. II(a) formation of colloidal crystal layer at the top surface; II(b) generation of small pores in the center of the polymer spheres; II(c) formation of open cells at the top layer; II(d) final porous film.

increased with the curvature of the air-solvent menisci, and finally with the evaporation rate, then, higher evaporation rate could cause stronger convective flow and more accumulation of nanoparticles. Thus, this gradual increase of evaporation rate, on the one hand, resulted in the gradual increase of silica particles migrating to the top surface along the radius from the center to the edge. On the other hand, this gradual increase of evaporation rate might cause the diffusion rate gradient of polymer chain, which finally behaved a gradual increase of deformation and coalescence degree of polymer spheres from the center to the edge of the film. The syntactic effect of silica particle migration and polymer diffusion caused gradient microstructures on the surface (see Fig. 10Ib, 10Ic and 10Id). A control experiment with pure polymer latex dried at 40 °C for 2 h, did not show any morphological evolution, further confirming the importance of colloidal silica particles, which formed a network via filling the interstitial spaces between the polymer spheres.

However, when the nanocomposite latex was dried at relatively high temperature, e. g., 110 °C, the temperature was so high that the central region had a comparable evaporation rate to the edge. As solvent evaporated, the concave capillary bridge between particle pairs, e.g., polymer spheres and silica particles played a significant role in pulling the particles together in order, while the conventional colloidal forces such as electrostatic repulsion forces granted the mobility of the spheres during the assembly [35]. Thus the polymer spheres self-assembled quickly into colloidal crystal fragments [36] which then impinged to form the first layer of the ordered packed structure on the top surface. Simultaneously the small silica beads were transferring through channels among the spheres in the consolidated layer to the evaporating menisci at the surface, and accumulating and filling in the interspaces between spheres, as shown in Fig. 10II a. On another hand, since the polymer has a far lower surface free energy (37.6 mJ/m^2) than silica (103.3 mJ/m^2), and the residual water or other medium in the latex spheres remarkably decrease the T_g of polymer [37], both could consequently make polymer chains easily diffuse cross boundary of spheres and fill into the voids and interstices between the silica beads, and cover the top layer of the film as well. As a result, the silica particles were embedded in the polymer chains, and the small pores were generated in the center of the polymer spheres (see Fig. 10IIb) [30]. As the diffusion of polymeric chains continued, the pore became larger and the wall of the pores thinner and finally, the open cells formed at the top layer of the film (see Fig. 10IIc). As the solvent continued to evaporate, the second layer of spheres assembled under the first layer with silica particles filling in the interspaces, and the diffusion of the polymer chains generated pores in the center of the polymer spheres as the first layer of ordered porous structure formed. As the free surface of the wet film descended towards the substrate, the pores formed layer by layer, and finally the three-dimensional ordered porous structure was built, as shown in Fig. 10IId.

4. Conclusions

Based on this study, a morphological gradient surface can be successfully fabricated via the film-formation of nanocomposite polymer dispersions at relatively low drying temperatures, neither careful experimental control nor any complex processes are needed. Both the T_g of polymer and the drying temperature have significant influences on the surface morphology. The nanocomposite dispersions from relatively low T_g of polymer can easily form morphological gradient surface during dried at room or a little bit higher temperatures, while the dispersions from relatively high T_g of polymer can not. When dried at high temperature, e.g., 110 °C, all the nanocomposite dispersions from both low and high T_gs of polymers cause three-dimensional porous films, no morphological gradient surface is obtained. This variation in surface morphology is ascribed to the different film-formation mechanism: the film-forming at relatively low temperatures mainly obeys the convective self-assembly mechanism, while the drying at high temperature hews to the air-solvent interface self-assembly mechanism.

This approach presents a new strategy in the preparations of morphological gradient on polymer surfaces, and is expected to fabricate other morphological gradient surface with functional organic and inorganic components. The gradient surface can be used to investigate protein adsorption, cell attachment and growth, nano-tribology, or combinational experiment. Related investigation is going under way.

Acknowledgements

Financial supports from the Foundation of Science and Technology of Shanghai (07DJ14004, 0952nm01000), Shanghai-Unilever Research and Development Fund (07su07001), the NSF (No. 20774023), the Shanghai Leading Academic Discipline Project (B113), the Shanghai Excellent Leader of Academic Discipline Project, and the Shuguang Scholar-Tracking Foundation of Shanghai are appreciated.

References

[1] Daniel S, Chaudhury MK, Chen JC. Science 2001;291:633.
[2] Morgenthaler S, Zink C, Spencer ND. Soft Matter 2008;4:419.
[3] Kim MS, Khang G, Lee HB. Prog Polym Sci 2008;33:138.
[4] Plummer ST, Wang Q, Bohn PW, Stockton R, Schwartz MA. Langmuir 2003;19:7528.
[5] Lee JH, Lee SJ, Khang G, Lee HB. J Colloid Interface Sci 2000;230:84.
[6] Zaari N, Rajagopalan P, Kim SK, Engler AJ, Wong JY. Adv Mater 2004;16:2133.
[7] Zhang J, Han Y. Langmuir 2008;24:796.
[8] Morgenthaler S, Lee S, Zürcher S, Spencer ND. Langmuir 2003;19:10459.
[9] Wu T, Efimenko K, Vlček P, Šubr V, Genzer J. Macromolecules 2003;36:2448.
[10] Sehayek T, Vaskevich A, Rubinstein I. J. Am Chem Soc 2003;125:4718.
[11] Chaudhury MK, Whitesides GM. Science 1992;256:1539.
[12] Liedberg B, Tengvall P. Langmuir 1995;11:3821.
[13] Jeong BJ, Lee JH, Lee HB. J Colloid Interface Sci 1996;178:757.
[14] Lee HB, Kim MS, Cho YH, Khang G. Polymer 2005;29:423.
[15] Dertinger SKW, Jiang X, Li Z, Murthy VN, Whitesides GM. Proc Natl Acad Sci U.S.A 2002;99:12542.
[16] Dalby MJ, Gadegaard N, Tare R, Andar A, Riehle MO, Herzyk P, et al. Nat Mater 2007;6:997.
[17] Vikhorev PG, Vikhoreva NN, Sundberg M, Balaz M, Albet-Torres N, Bunk R, et al. Langmuir 2008;24:13509.
[18] Fuierer RR, Carroll RL, Feldheim DL, Gorman CB. Adv Mater 2002;14:154.
[19] Genzer J, Bhat RR. Langmuir 2008;24:2294.
[20] Genzer J, Efimenko K, Fischer DA. Langmuir 2006;22:8532.
[21] Xu C, Wu T, Drain CM, Batteas JD, Fasolka MJ, Beers KL. Macromolecules 2006; 39:3359.
[22] Tsai IY, Kimura M, Russell TP. Langmuir 2004;20:5952.
[23] Lu X, Zhang J, Zhang C, Han Y. Macromol Rapid Commun 2005;26:637.
[24] Zhang J, Xue L, Han Y. Langmuir 2005;21:5.
[25] Kunzler TP, Drobek T, Sprecher CM, Schuler M, Spencer ND. Appl Surf Sci 2006;253:2148.
[26] Blondiaux N, Morgenthaler S, Pugin R, Spencer ND, Liley M. Appl Surf Sci 2008;254:6820.
[27] Washburna NR, Yamada KM, Simon CG, Kennedy SB, Amis E. Biomaterials 2004;25:1215.
[28] You B, Wen N, Zhou S, Wu L, Zhao D. J Phys Chem B 2008;112:7706.
[29] You B, Shi L, Wen N, Liu X, Wu L, Zi J. Macromolecules 2008;41:6624.
[30] Zhang S, Zhou S, You B, Wu L. Macromolecules 2009;42:3591.
[31] Zeng F, Sun Z, Wang C, Ren B, Liu X, Tong Z. Langmuir 2002;18:9116.
[32] Kralchevsky PA, Denkov ND. Curr Opin Colloid Interface Sci 2001;6:383.
[33] Tirumkudulu MS, Russel WB. Langmuir 2004;20:2947.
[34] Deegan RD, Bakajin O, Dupont TF, Huber G, Nagel SR, Witten TA. Nature 1997;389:827.
[35] Dimitrov AS, Nagayama K. Langmuir 1996;12:1303.
[36] Stamou D, Duschl C, Johannsmann D. Phys Rev E 2000;62:5263.
[37] Song M, Hourston DJ, Silva GG, Machado JC. J Polym Sci Part B Polym Phys 2001;39:1659.